J. Fluid Mech. (1989), *vol.* 203, *pp.* 173–197
Printed in Great Britain

Pulsatile flow through constricted tubes: an experimental investigation using photochromic tracer methods

By MATADIAL OJHA,[1] RICHARD S. C. COBBOLD,[1] K. WAYNE JOHNSTON[1] AND RICHARD L. HUMMEL[2]

[1] Institute of Biomedical Engineering, University of Toronto, Toronto M5S 1A4, Canada
[2] Department of Chemical Engineering, University of Toronto, Toronto M5S 1A4, Canada

(Received 27 April 1988)

A photochromic tracer method has been used to record pulsatile flow velocity profiles simultaneously at three axial locations along a flow channel. Two major advantages of this multiple-trace method are that it enables velocity data to be acquired in an efficient non-invasive manner and that it provides a detailed description of the spatial relationship of the flow field. The latter is found to be particularly useful in the investigation of transitional type flows; for example, in describing coherent flow structures. Studies of the flow patterns in tubes with mild to moderate degrees of vessel constriction were performed using a 2.9 Hz sinusoidal flow superimposed on a steady flow (frequency parameter of 7.5; mean and modulation Reynolds numbers of 575 and 360, respectively). With mild constrictions (< 50% area reduction), isolated regions of vortical and helical structures were observed primarily during the deceleration phase of the flow cycle and in the vicinity of the reattachment point. As expected, these effects were accentuated when the constriction was asymmetric. For moderate constrictions (50%–80%), transition to turbulence was triggered just before peak flow through the breakdown of waves and streamwise vortices that were shed in the high-shear layer. During this vortex generation phase of the flow cycle, the wall shear stress fluctuated quite intensely, especially in the vicinity of the reattachment point, and its instantaneous value increased by at least a factor of eight. Such detailed descriptions of the transition to turbulence and of the spatial and temporal variation of the wall shear stress, particularly near the reattachment point, have not been previously reported for pulsatile flow through constricted tubes. The observed wall shear stress variations support a proposal by Mao & Hanratty (1986) of an interaction of the imposed flow oscillation with the turbulent fluctuations within the viscous sublayer.

1. Introduction

Because of its relevance to a number of engineering and biological systems, there has been a considerable interest in the dynamics of pulsatile pipe flow (Shemer, Wygnanski & Kit, 1985; Stettler & Hussain 1986; Mao & Hanratty 1986). For instance, in the biomedical field, pulsating flows have been studied primarily to understand the changes to the blood flow pattern due to constrictions or stenoses (Ahmed & Giddens 1984), bends and bifurcations (Ku & Giddens 1987) and aortic valve prostheses (Yoganathan, Corcoan & Harrison 1979; Hanle *et al.* 1987), and also to assess the potential clinical use of high-frequency ventilator systems for use during surgery and in intensive care (Gaver & Grotberg 1986).

Our work was motivated by the need for an improved understanding of the effects of stenoses (constrictions), especially moderate to minor stenoses, on arterial blood flow patterns. It is well known that for an arterial cross-sectional area reduction of around 80%, the mean volumetric flow is significantly reduced and that turbulence is generally triggered. The flow disturbances associated with severe stenoses can be detected non-invasively through the use of Doppler ultrasound spectral analysis (Barnes *et al.* 1976; Johnston *et al.* 1986). The detection and quantitative assessment of less severe stenoses, particularly minor stenoses ($< 50\%$ area reduction), is also of great importance since it can probably allow appropriate drug or dietary treatment at an early stage of disease progression. However, progress in non-invasive diagnosis of minor stenoses has been slow, and this is partially attributable to the lack of detailed knowledge concerning the hemodynamics of pulsatile flow through stenosed vessels. An improved understanding of pulsatile flow through constricted tubes might well lead to better interpretation of Doppler ultrasound spectra, thereby enhancing the ability to quantitatively assess moderate and minor degrees of stenosis. Furthermore, in view of evidence that hemodynamic factors could contribute to the progression of arterial disease (Ku & Giddens 1987), the results could be important in understanding possible mechanisms.

For pulsatile flow through straight tubes, Stettler & Hussain (1986) have presented a detailed discussion of the transition to turbulence. Of particular significance is the introduction of a set of three non-dimensional parameters that characterize the flow when the driving force consists of a mean plus a single sinusoidal component. Specifically, they determined the laminar-transition criteria in terms of a mean Reynolds number (Re_{m}), a modulation Reynolds numer ($Re_{\mathrm{m}\omega}$) and a frequency parameter α. These quantities are defined by

mean Reynolds number	$Re_{\mathrm{m}} = U_{\mathrm{m}} D/\nu,$
modulation Reynolds number	$Re_{\mathrm{m}\omega} = U_{\mathrm{m}\omega} D/\nu,$
frequency parameter	$\alpha = D/2(\omega/\nu)^{\frac{1}{2}},$

where D is the tube diameter, ν is the kinematic viscosity, ω is the angular frequency, U_{m} is the time-mean of the average cross-sectional velocity, and $U_{\mathrm{m}\omega}$ is half the peak–peak amplitude of the average cross-sectional velocity waveform. In examining flows at around the transitional Reynolds number, they found that for various combinations of Re_{m} and $Re_{\mathrm{m}\omega}$, maximum stability occurred at $\alpha \approx 5$. Of importance are their observations that turbulent patches were generated by the sinusoidal flow component and that they differed in structural detail from the turbulent puffs or slugs normally seen in steady flow. These patches occurred at random or were phase-locked depending on the values of the flow parameters. This new phenomenon was used to explain previous reports of turbulence during the deceleration phase of the flow cycle followed by relaminarization during the acceleration phase (Hino, Sawamoto & Tokasu 1976; Ramaprian & Tu 1980).

The effect of periodic oscillations on the time-averaged velocity profile and wall shear stress have been investigated by Shemer *et al.* (1985). They concluded that for $\alpha = 4.5$, $Re_{\mathrm{m}} = 4000$ and $Re_{\mathrm{m}\omega} = 1800$, the periodic oscillations have no significant effect in either the laminar or turbulent flow regimes. However, Ramaprian & Tu (1980, 1983) found that for sufficiently high frequencies, in which the timescale of the unsteadiness was comparable with that of the turbulent eddies, the time-mean velocity profile was affected and the time-mean wall shear stress and power loss due to friction were both increased. Their work indicates that a quasi-steady turbulence

model cannot adequately describe unsteady flow conditions, at least for high frequencies.

Experimental studies on pulsatile flow through constricted tubes using laser Doppler anemometry as well as flow visualization using hydrogen bubble and dye injection methods have yielded some significant results (Ahmed & Giddens 1984; Lieber 1985). Our study employs the photochromic tracer method (Smith & Hummel 1973) which simultaneously allows the flow to be visualized and permits the measurement of the instantaneous velocity profiles. Furthermore, it can provide quantitative information in both the Eulerian and Lagrangian frames of reference (Dunn & Smith 1972; Davis *et al.* 1985). As will be seen, the method is of considerable value in characterizing pulsatile flow through constrictions; it can also provide a valuable means for characterizing coherent structures such as turbulent patches (Stettler & Hussain 1986; Hussain 1986) and turbulent bursts (Talmon, Kunen & Ooms 1986).

The overall purpose of our work was to investigate pulsatile flow patterns created by mild to moderate degrees of constriction using flow conditions that approximately correspond to those seen in a medium sized artery such as the internal carotid artery. Specifically, we made use of a split-beam photochromic tracer method that allows dye traces to be recorded simultaneously at three locations, thereby enabling the time and spatial distributions of the wall shear stress to be studied, as well as visualizing the flow. In addition, we studied the transition to turbulence triggered by the moderate stenoses. We believe that the methods used and results obtained are of general interest, and it is from this perspective that an overall evaluation of the technique is also presented.

2. Experimental

2.1. *Photochromic tracer method*

The photochromic tracer method makes use of the properties of a normally colourless indicator in the test fluid. Upon irradiation with UV light the indicator undergoes a reversible photochemical reaction resulting in a colour change. The trace produced by a pulsed UV laser is photographed at a selected time after its formation, thereby enabling the average velocity within the time interval to be obtained. It was the first method to show the existence of the viscous sublayer in turbulent pipe flow and to reveal tht the normalized thickness (y^+) of the viscous sublayer oscillates and can be much smaller than the previously accepted value of $y^+ = 5.0$ (Popovich & Hummel 1967). Here $y^+ = y(\tau_W/\rho)^{\frac{1}{2}}/\nu$, where y is the actual thickness of the sublayer, τ_W is the wall shear stress and ρ is the fluid density. This finding has led to more accurate modelling of heat and mass transfer processes (Thomas 1980). The method has also been applied quite successfully in other steady flow investigations (Iribarne *et al.* 1969, 1972; Seeley, Hummel & Smith 1975; Kondratas & Hummel 1980).

Initial work on the application of the photochromic tracer method for the study of pulsatile flow has shown good promise (Poots *et al.* 1986*a*, *b*). However, in this earlier work the spatial resolution was not sufficient to allow detailed flow examination. Recently, improvements have been made (Ojha 1987; Ojha *et al.* 1988) and these have resulted in the trace width being reduced from 1.2 to 0.2 mm with better defined trace boundaries, giving an eight-fold or greater overall improvement in spatial resolution. The results that can be achieved are illustrated in figure 1, which shows a sequence of traces at 40 ms intervals throughout a 2.9 Hz sinusoidal flow in a straight tube. Each trace (velocity profile) was recorded 5.1 ms following its

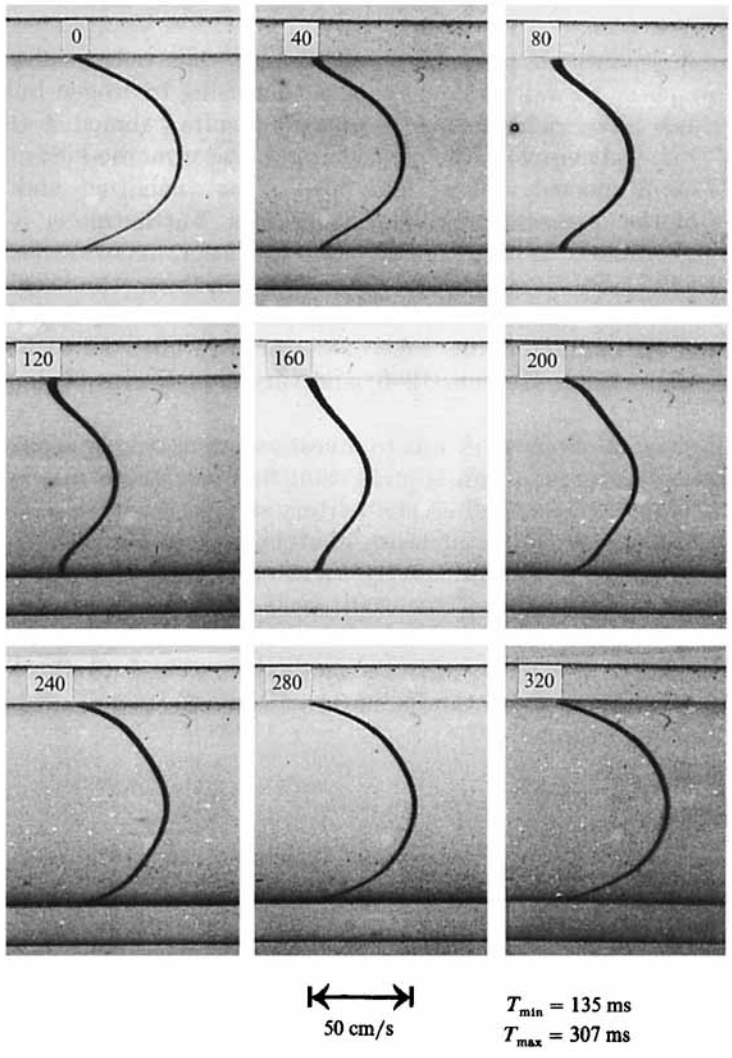

FIGURE 1. Displacement profiles of the dye traces photographed 5.1 ms after their formation in a tube of 5.1 mm ID. The profiles represent the axial velocity profiles seen at 40 ms intervals throughout a flow cycle consisting of a 2.9 Hz sinusoidal flow superimposed on a steady flow. The entry point of the laser beam is on the upper wall for each frame: the same is true for all the subsequent photographs.

formation. Careful inspection of this figure shows a small asymmetry in the dye displacement profiles that arises from the fact that the laser beam was not exactly incident at 90°. This misalignment poses no problem since it is the net displacement at any radial position that is used in determining the velocity profile.

2.2. *Apparatus and methods*

The computer-controlled measurement system used in our experiments is illustrated in figure 2. Details of the system, which is an improvement of the original system described by Poots *et al.* (1986*a*), are presented elsewhere (Ojha 1987; Ojha *et al.* 1988). In essence, it consists of a pulsed nitrogen laser, a mechanical pump flow synthesizer, a 35 mm camera and electronic flash, a flow test section and optics, and

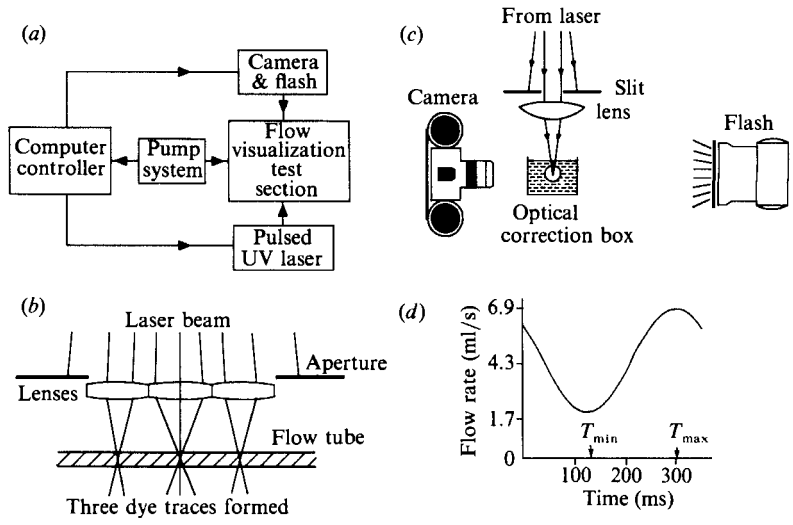

FIGURE 2. Schematic representations of (*a*) the major components of the measurement system; (*b*) longitudinal view showing the lens arrangement for the formation of multiple traces (note, the focal length of the lenses are 10 cm and the aperture width is 2.4 cm, so that the beam divergence is much less than that illustrated); (*c*) cross-sectional view of the test and optical systems; (*d*) volumetric flow waveform whose period is 345 ms.

a microcomputer controller. The computer controller provides precise timing, enabling the photochromic dye traces to be photographed at selected intervals within a flow cycle using delays of 5.1 ms or less after their formation. In order to generate the pulsatile flow waveform the output of a 2.9 Hz piston pump was superimposed on that of a steady flow gear pump. Deoderized kerosene (Shell-Sol 715) that has a density of 0.755 g/cm^3 and a viscosity of 1.43 cP at 20 °C was used as the test fluid. The flow section consisted of a 1.2 m long glass tube of approximately 5.0 mm inside diameter. The test section was located 160 diameters downstream from the entrance and, as shown in figure 2*c*, an optical correction box is used to reduce distortion. For a tube diameter of 5.0 mm ID, these conditions correspond to a mean and modulation Reynolds numbers of 575 and 360, respectively, and a frequency parameter of 7.5: values that are similar to those found in the human internal carotid artery. The flow waveform is shown in figure 2(*d*): the period is 345 ms and the times $T_{min} = 135$ and $T_{max} = 307$ are the instants of minimum and maximum flow.

The photochromic solution consisted of 0.01 % by weight of the indicator 1′,3′,3′-trimethylindoline-6-nitrobenzospiropyran (TNSB) dissolved in Shell-Sol 715. Such a low concentration does not affect the physical properties of the solvent, but the concentration is sufficient to ensure that a fairly uniform trace with satisfactory contrast is produced across the Pyrex tube. A dark blue trace develops in less than 10^{-6} s following the laser discharge (duration $< 10^{-8}$ s). The trace is photographed at a selected time after its formation on Kodak Technical Pan 2415 film through the use of a Nikon-F 35 mm SLR camera equipped with a 55 mm Nikon micro lens and a Vivitar 285 flash. This selected time will be referred to as the flash delay and it actually represents the time interval between the triggering of the nitrogen laser and the discharge of the Vivitar flash. Best contrast in photographing the blue dye trace is achieved using green light. This was achieved by using a green dichroic filter on the flash and a yellow filter on the camera. It should also be noted that the sampling

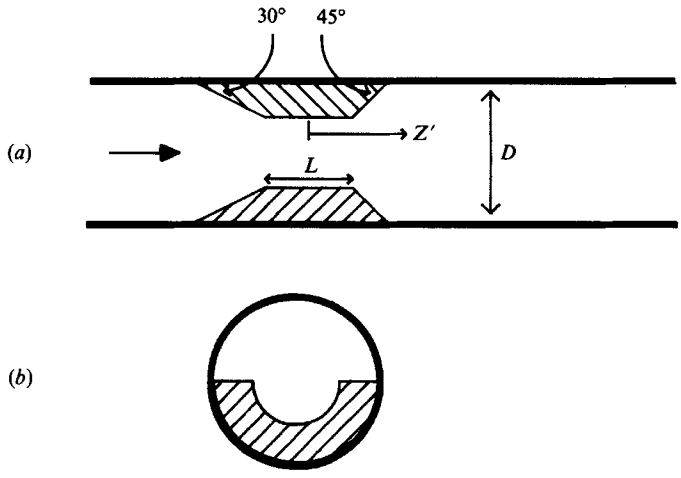

FIGURE 3. Geometry of stenoses used in the experiments. (*a*) Axisymmetric. (*b*) Asymmetric: the plan view is the same as (*a*). For both types of stenoses $L = 1.5$ mm and $D = 5.0$ mm. The normalized distance from the centre of the stenosis is given by $Z = Z'/D$.

nature of the method allows only one picture or sample to be taken in any given cycle. Normally, 20 pictures are taken at times that are equivalent to 20 ms intervals throughout the flow cycle.

Both axisymmetric and asymmetric stenoses, whose geometries are shown in figure 3, were investigated. Based on our clinical observations, their orientation and size are similar to those found *in vivo*. For the axisymmetric stenoses the maximum percentage cross-sectional area reductions are 45, 65 and 75%, while for the asymmetric stenosis it is 38% (of the total cross-sectional area). They were made from clear Plexiglas acrylic rods and were machined such that the fit was tight in each of the Pyrex glass tubes and their edges were polished. Each stenosis was held securely inside the tube through the use of a low-viscosity cyanoacrylate gluc that was poured through holes drilled in the tube walls.

In order to observe the transition to turbulence in more detail for the 75% stenosis, the motion of the downstream separation boundary was followed by continuously generating the coloured form of the photochromic indicator in the separation region. This was accomplished by placing a 100 W mercury lamp (Phillips CS 100 W) about 0.8 m from the test section and using a 10 cm focal length lens to focus the light onto the tube wall. Also, the concentration of the indicator was increased to 0.04% by weight to ensure that virtually all the incident UV light was absorbed in the separation region. The dye streaks were photographed by the 35 mm SLR camera and also by a 16 mm Locam movie camera equipped with a 50 mm Canon Macro lens, using a frame rate of 400/s. Background illumination for the movies was provided by a sodium lamp (GE 400 W, Lucalox).

3. Results

3.1. *Errors*

A detailed discussion of the measurement and analysis errors associated with the photochromic tracer method has been presented elsewhere (Ojha *et al.* 1988). It was shown that for a one-dimensional flow through a 5 mm tube diameter and with a flash delay of 5.1 ms, the error in the velocity u was $\pm[0.15^2 + (0.015\,u)^2]^{\frac{1}{2}}$ cm/s, e.g.

for a velocity of 60 cm/s, the error is ± 0.9 cm/s. For the more complex flow patterns, as seen downstream from a stenosis, much larger errors can occur and these depend on the flash delay and the timescale of the turbulent eddies. In general, evaluation of these errors is difficult; however, in regions of strong secondary flows or turbulence, the main emphasis of this paper is on the measurement of the wall shear stress. Since it was found that in the viscous sublayer vortices were absent and radial flow was very small, the measurement error arising from these phenomena was assumed to be negligible.

Our experiments with the moderate stenoses show the location of the reattachment point shortly after peak flow to be a chaotic region with a negative radial pressure gradient, and to have considerable axial and radial accelerations. We found that for delays of 5.1 ms significant blurring of the traces occurred due to the chaotic nature of the flow. Shorter delays of 2.1 and 1.1 ms reduced this blurring and resulted in more accurate values. Furthermore, it should be noted that if the acceleration during the interval between the trace formation and the photograph is large, then the effects of averaging will be significant. This effect was considerably reduced by using the shorter flash delays. Since the means and variances of the data obtained with the shorter delays were similar, it was assumed that these were short enough to greatly reduce acceleration effects.

Measurements of the wall shear stress were performed by curve fitting the digitized trace segment closest to the wall. Based on our previous results (Ojha *et al.* 1988), our best estimate of the error in measuring the wall shear stress (τ_W for a flash delay of 1.1 ms is $\pm[(0.06\tau_W)^2 + (0.5)^2]^{\frac{1}{2}}$ dynes/cm^2. For instance, if $\tau_W = 50$ dynes/cm^2 the error is ± 3 dynes/cm^2, while if $\tau_W = 0$ the error is ± 0.5 dynes/cm^2.

3.2. *Mild stenoses*

We define a mild stenosis to be one that results in turbulence in isolated regions, as opposed to turbulence that occupies the entire vessel cross-section. Both the 38% asymmetric and the 45% axisymmetric stenoses fall into this category. The fact that mild stenoses are generally asymmetric *in vivo* prompted the investigation of such a shape. In order to obtain good flow resolution a flash delay of 5.1 ms was chosen. Selected photographs of the dye displacement profiles at 60 ms intervals throughout the flow cycle are shown in figure 4. In fact, these profiles represent the axial velocity distributions. The centreline velocity waveforms measured at various downstream locations are shown in figure 5. With the 45% stenosis, the sinusoidal nature of the flow is seen at all three locations. During the latter portion of the cycle the flow acceleration is significanlty greater close to the stenosis at $Z = 1.0$ (Z = number of tube diameters from the centre of the stenosis). This is because the effect of this mild stenosis, as reflected by the jet flow and the associated reverse flow, is more pronounced in the near poststenotic region. However, with the 38% asymmetric constriction, the smooth sinusoidal variation was only observed close to the stenosis. Further downstream, as displayed in the photographs of figure 4, the asymmetry of the 38% occlusion affects the flow pattern quite strongly: for example, the centreline velocity does not always represent the peak velocity. Also, in the vicinity of the reattachment point and during the deceleration phase of the flow cycle, substantial fluctuations of the axial velocity are present over a major portion of the vessel cross-section. The fluctuation of the axial velocity with the downstream position Z is greater for the asymmetric (38%) than that for the axisymmetric (45%) stensosis, and, as follows from the continuity equation, this indicates greater non-axial velocities.

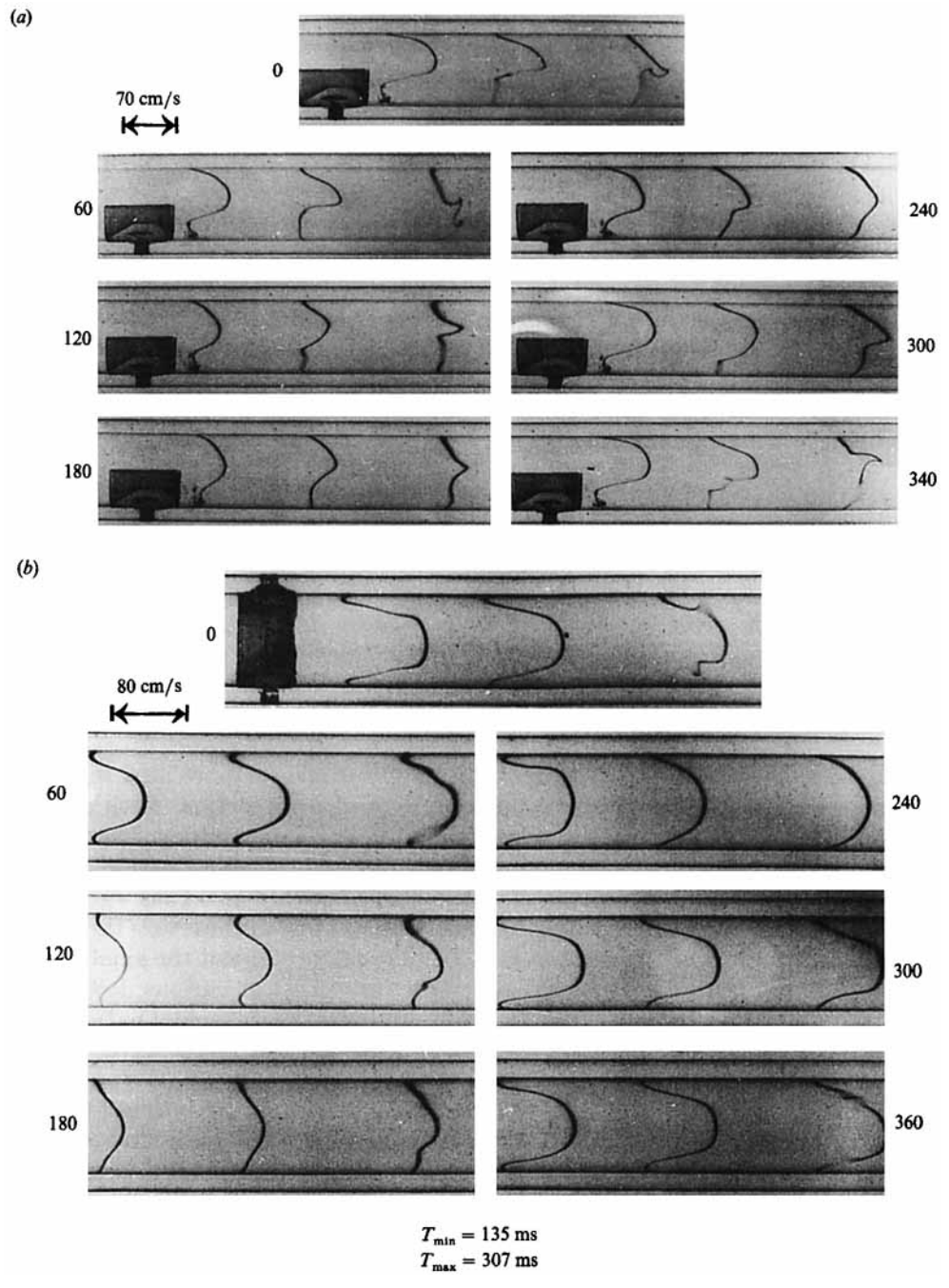

FIGURE 4. Selected photographs at the indicated times throughout the flow cycle for (*a*) the 38% asymmetric stenosis, with the traces positioned at $Z = 0.7$, 2.2 and 4.0; (*b*) the 45% axisymmetric stenosis at $Z = 1.0$, 2.5 and 4.3.

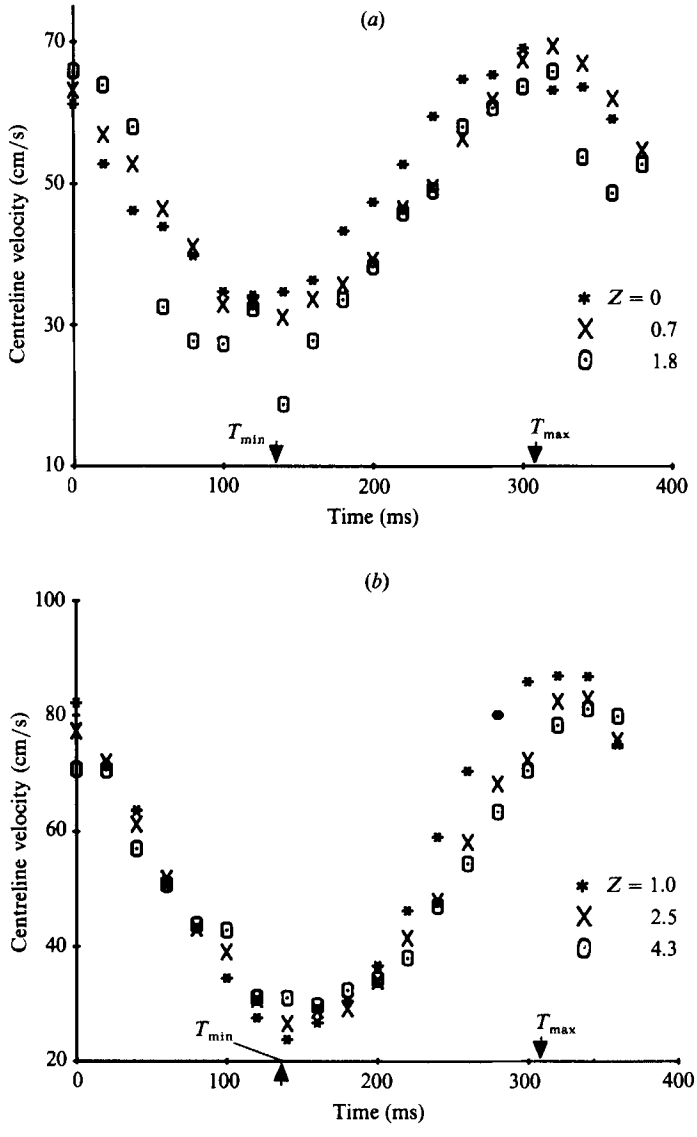

FIGURE 5. Centreline velocity waveforms at the indicated axial locations for (*a*) the 38% asymmetric stenosis; (*b*) the 45% axisymmetric stenosis.

The position of the reattachment point is known to be very susceptible to small disturbances. Consequently, should the flow become unstable, it would be expected that the effects of the instability would be first observed at and around the reattachment point, and this would be especially pronounced during the early part of the deceleration phase in the flow cycle. This behaviour is illustrated in figure 4 where it can be seen that the instability leads to the formation of highly localized eddies and transverse ejections (see frames 0 and 60) along with the associated high shear rates. The instability often occurs at sites where the velocity profiles appear to be highly inflectional and is more pronounced for the 38% asymmetric constriction, probably due to the tendency of the jet to drift towards the stenosed-side of the vessel.

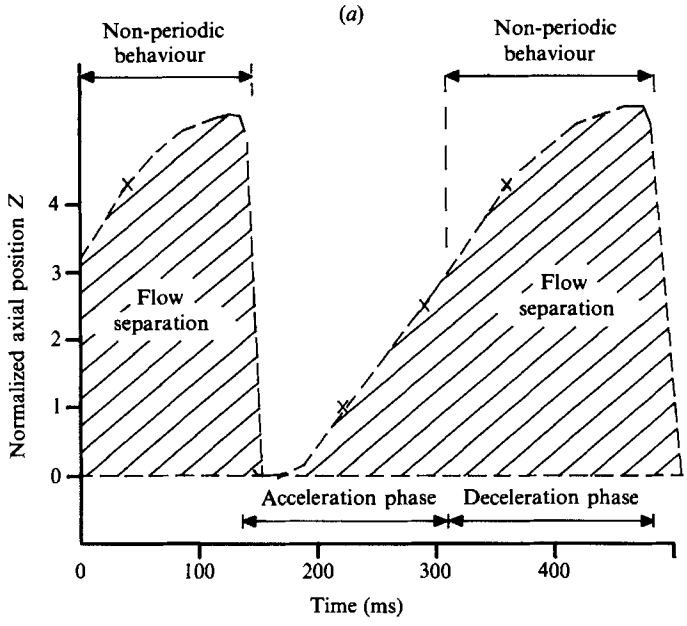

FIGURE 6(a). For caption see facing page.

The flow separation pattern can be easily followed through the use of multiple traces and by simply observing the near-wall velocity profiles. The reattachment point oscillates over quite a large distance during the pump cycle. For example, figure 6(*a*) shows the approximate movement of the reattachment point for the 45% axisymmetric stenosis, based on the observations made at the three axial locaions. As the flow starts to accelerate it moves rapidly upstream from beyond $Z = 4.3$ towards the stenosis. Approximately 80 ms into the acceleration phase ($t = 220$ ms) the reattachment point moves downstream past $Z = 1.0$ towards $Z = 2.5$ and eventually reaches $Z = 4.3$ at about 60 ms into the deceleration phase. Figure 6(*b*) shows the variation in the normalized (to the tube radius) thickness of the separation zone at three axial locations for both tube walls throughout the flow cycle. The symmetric (across the tube axis) waveform shows a gradual increase in thickness during the deceleration phase of the flow cycle followed by an abrupt decrease to zero just after the start of the acceleration phase. The abrupt change seen at $Z = 2.5$ and 4.3 during the deceleration phase appears to arise from enhancement of the flow instability around the reattachment point, as discussed earlier.

A different flow separation pattern is observed with the 38% asymmetric constriction. Figure 7 shows time variation of the separation zone thickness at $Z = 0.7$ and 1.8. Along the stenosed-side of the vessel at $Z = 0.7$, flow separation was present throughout the flow cycle. The gradual increase during the deceleration phase followed by the decrease as the flow accelerates ($t = 140$ ms) is similar to that seen with the 45% axisymmetric stenosis. However, further downstream at $Z = 1.8$ a strong non-cyclic fluctuation of the separation boundary is seen during the deceleration phase which continues into the early part of the acceleration phase. The profiles shown in figure 4(*a*), particularly the traces furthest downstream in frames 0, 20 and 340 ms, indicate that these effects are probably caused by the generation of waves, vortices and three-dimensional structures in the vicinity of the reattachment point with possible amplification by the tendency of the jet to drift

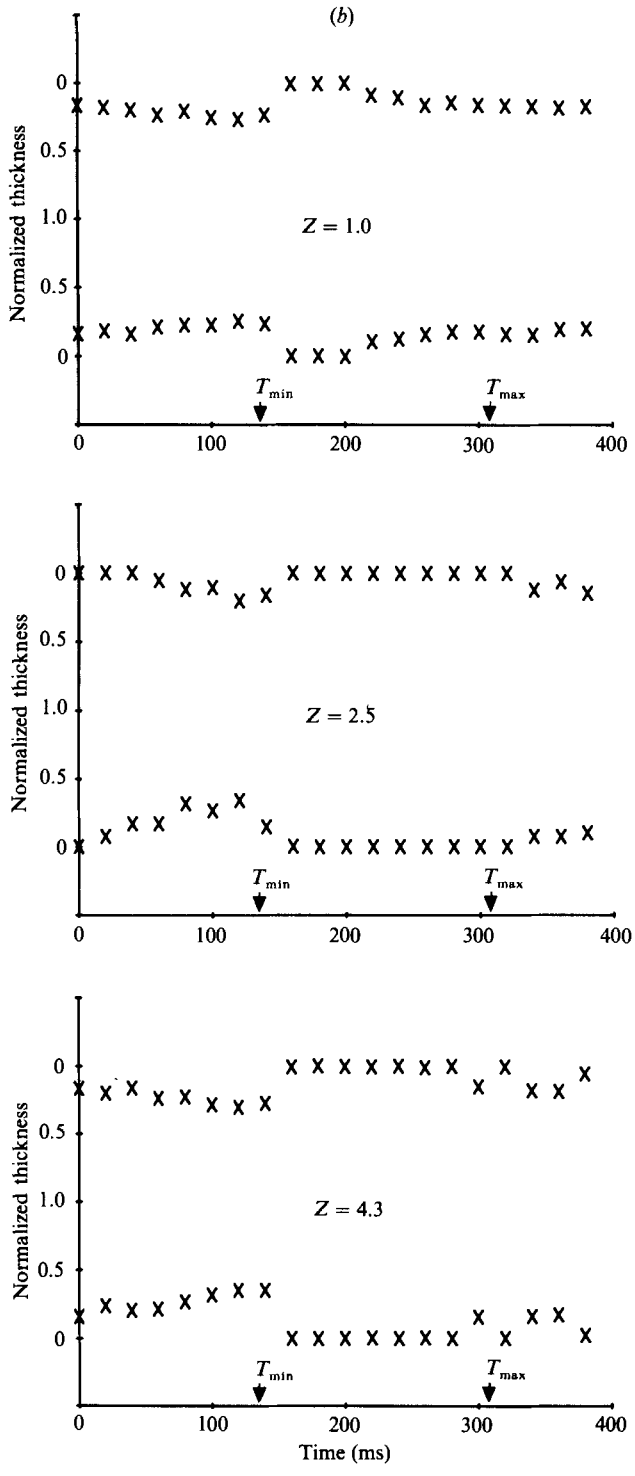

FIGURE 6. Time-dependent characteristics of the flow separation region for the 45% axisymmetric stenosis: (*a*) normalized axial position of the reattachment point; (*b*) normalized (to the tube radius) thickness of the separation region at three axial positions: for each graph, the lower profile is that associated with the vessel wall through which the laser beam enters.

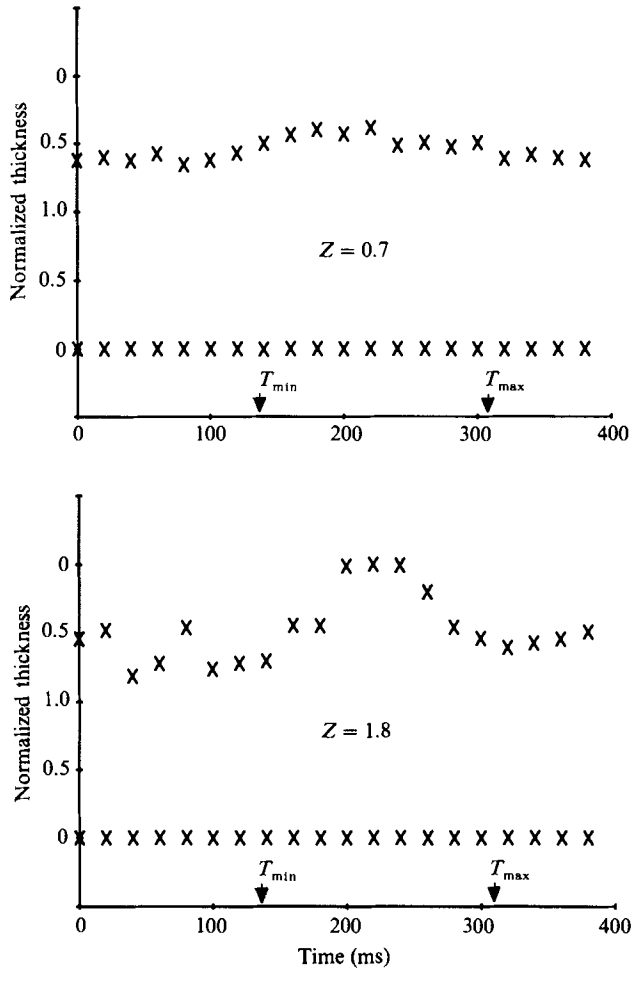

FIGURE 7. Variation of the normalized thickness of the separation region for 38% asymmetric stenosis.

towards the stenosed-side of the vessel. The reattachment point lies mostly between $Z = 0.7$ and 1.8 during the acceleration phase and between $Z = 1.8$ and 4.0 during the deceleration phase.

The time variation of the upstream wall shear stress for the 75% stenosis, which is typical for all the stenoses, is shown in figure 8. The two sets of data points correspond to the two walls where the trace intersects. The solid curve corresponds to the sinusoidal waveform predicted using the Womersley (1955) rigid-tube model: details are given elsewhere (Ojha *et al.* 1988). The mean value and range are 4.2 and -1.7 to 10.0 dynes/cm^2 respectively. It can be seen from the figure that the values for the two walls are in agreement to within the experimental error, and in addition there is good overall agreement with the theoretical profile, both in amplitude as well as phase. In addition, it was found that the wall shear stress leads the volumetric flow by about $31 \pm 4°$, which is close to the theoretical value of 36° (Ojha *et al.* 1988).

As shown in table 1, the wall shear stresses in the downstream region of the stenoses oscillate over a range of values that is different from the upstream region of the stenoses. For example, larger positive values occur at the exit of the 38%

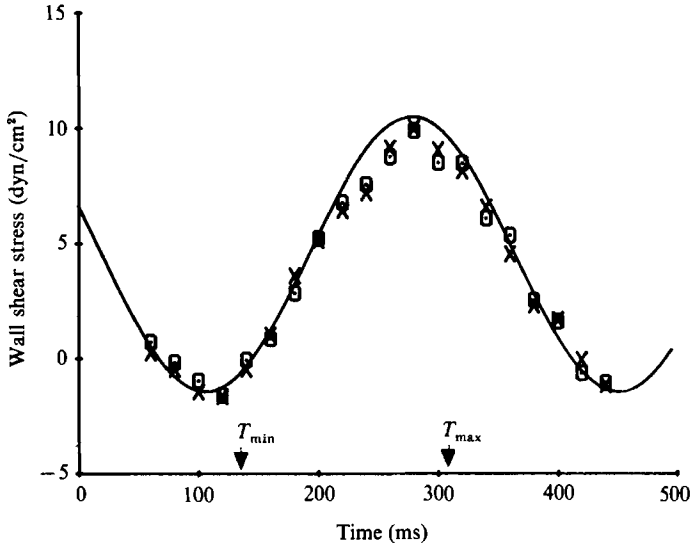

FIGURE 8. Measured time dependence of the wall shear stress upstream of the 75% stenosis for the upper (×) and lower (⊙) walls compared with the predicted profile (solid line). It should be noted that the measured wall shear stress waveform leads the volumetric flow waveform by about 31°.

		Shear stress (dynes/cm²)	
Stenosis	Z	Mean	Range
38%	0	16.0	4.3–32.5
	0.7	11.8	4.6–17.0*
	1.8		−0.2–8.6*
	4.0	1.6	−0.7–6.3
45%	1.0	−3.1	−6.3–3.0
	2.5	−0.8	−8.1–7.5
	4.3	2.0	−5.8–12.4

TABLE 1. Measured wall shear stresses (mean and range) obtained over a typical flow cycle at the indicated locations (Z) for the 38% and 45% stenoses. The asterisk indicates the value for unstenosed side of the vessel

asymmetric stenosis owing to the direction of the jet towards the unstenosed side of the vessel, and larger negative values occur between $Z = 2.5$ and 4.3 of the 45% stenosis owing to the increased reverse flow.

3.3. *Moderate stenoses*

We define a moderate stenosis to be one for which turbulence is generated across the entire vessel, but which does not result in a physiologically significant reduction in blood flow. Both the 65% and 75% stenoses fall in this category and the transition to turbulence is clearly shown in figures 9 and 10. In the jet regions of both stenoses, which extend to around $Z = 3.0$, the flow appeared to be quite stable and to be two-dimensional. Figure 11 shows that the centreline velocities in the jet regions exhibit a nearly sinusoidal variation. It should be noted that the displacement of the trace over the 5.1 ms flash delay is relatively large and consequently the measured velocity represents the time-averaged Lagrangian velocity.

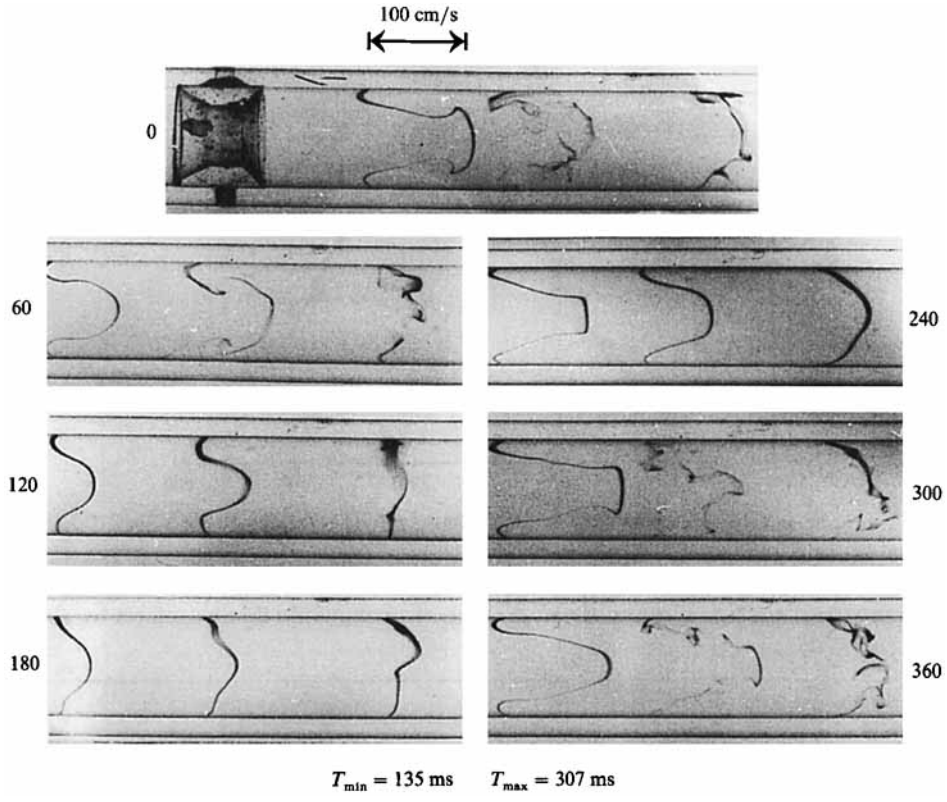

FIGURE 9. Selected photographs taken at 60 ms intervals throughout the flow cycle for the 65% axisymmetric stenosis. The flash delay was 5.1 ms, and the axial locations of the three traces are $Z = 1.5$, 3.0, and 4.8.

Variations in thickness of the separation zones in the stable jet region are shown in figure 12. They are similar to those observed with the mild stenoses at comparable locations. In addition, it was observed from the full set of photographs corresponding to figures 9 and 10, that the reattachment point fluctuates mostly within the range $Z = 3.0$ to 4.8, except that, during the early part of the acceleration phase when conditions are least favourable for flow separation, it moves upstream. While a permanent flow separation region was seen with the 75% stenosis, for the 65% stenosis only a transient flow separation region was apparent from the dye traces.

As mentioned earlier, the motion of the separation boundary of the 75% stenosis was followed by generating the coloured form of the photochromic indicator in the separation region. The dye streaks were photographed at selected points in the flow cycle using the 35 mm camera and, more importantly, in a continuous manner by the use of the movie camera operating at 400 frames/s. The photographs in figure 13, taken with the 35 mm camera, illustrate the separation boundary between the forward and reverse flows and the accumulation of the dye in the convergent section of the stenosis. The far-wall separation boundary is faintly visible, indicating some penetration of UV light to this region. With the movie camera, the dye was seen to circulate upstream towards the stenosis and was then swept downstream. Based on these observations, together with information from the laser/dye traces, we have constructed the set of frames shown in figure 14. The top frame represents the instant in the flow cycle at which all turbulence generated by direct breakdown of waves and

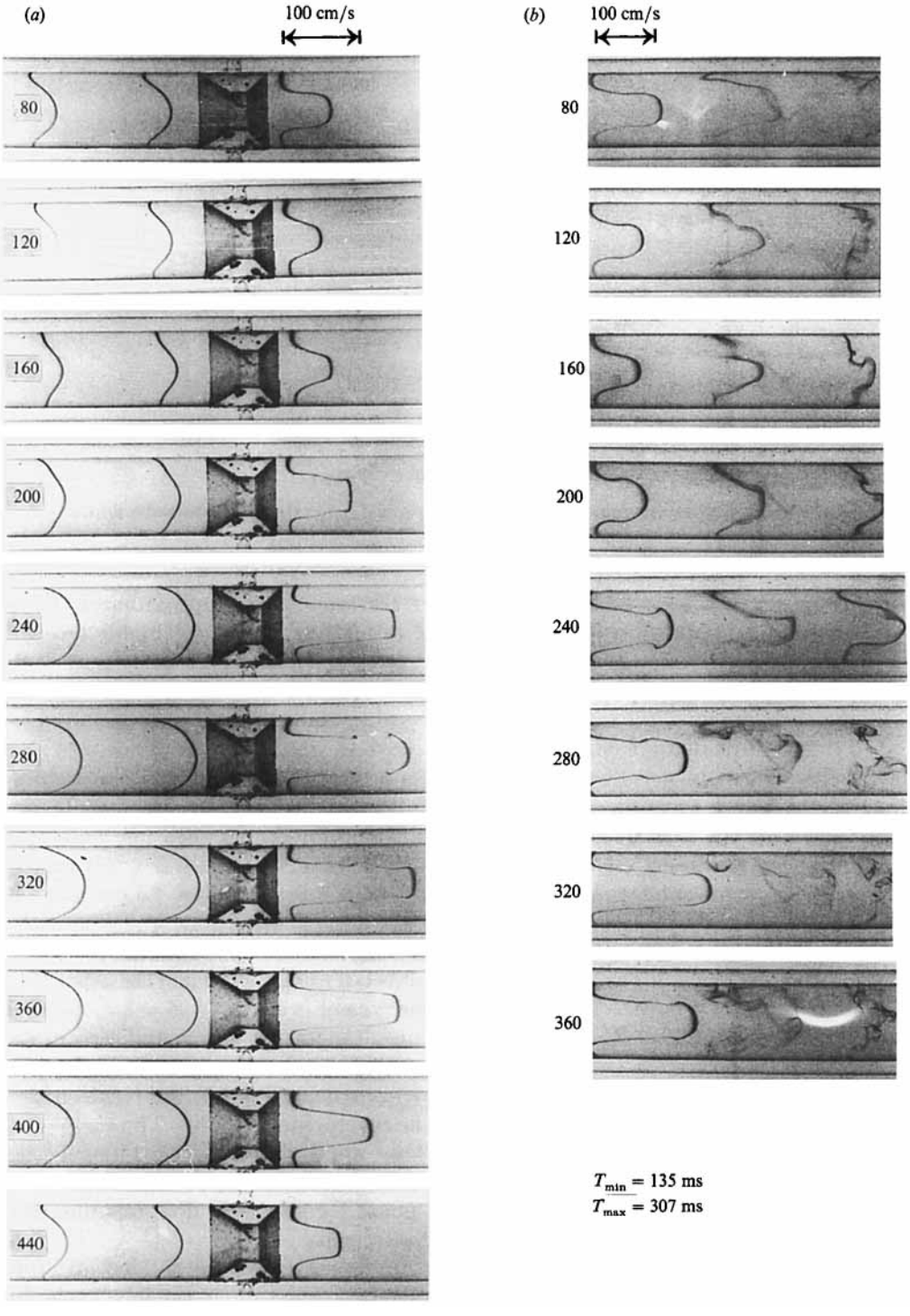

FIGURE 10. Selected photographs taken at 40 ms intervals throughout the flow cycle for the 75% stenosis. The flash delay was 5.1 ms, and the axial locations of the three traces are (*a*) $Z = -2.7$, -1.2, 0.6; (*b*) $Z = 1.2$, 2.8, 4.5. The two sets of photographs can be viewed as representing the flow field from $Z = -2.7$ to $Z = 4.5$, bearing in mind that each frame of three traces is from different cycles.

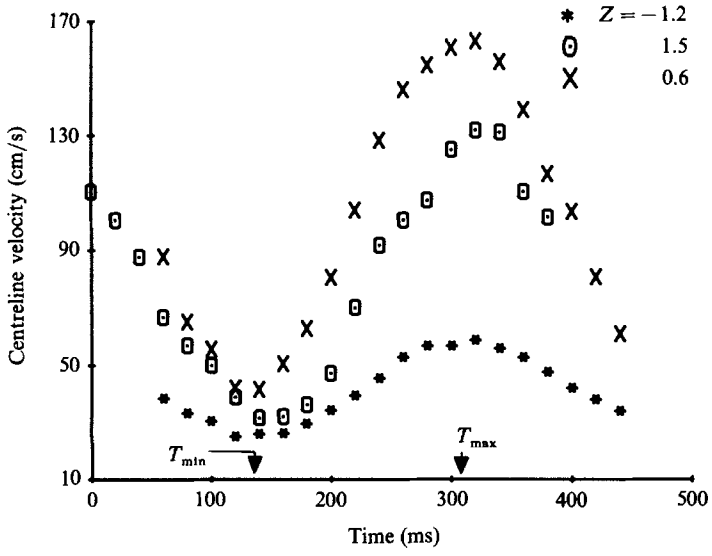

FIGURE 11. Centreline velocity waveforms at $Z = 1.5$ for the 65% stenosis, and at $Z = 1.2$ and 0.6 for the 75% stenosis.

streamwise vortices near $Z = 4.5$ ceases. This corresponds to approximately 60 ms before minimum flow ($T_{min} - 60$ ms). Beyond $Z = 4.5$ the flow was still highly unstable throughout the remainder of the deceleration phase and even in the early part of the acceleration phase. The reattachment point fluctuated around $Z = 4.5$ and the normalized thickness of the separation zone was about $0.38R$ (where $R = \frac{1}{2}D$) from the exit of the stenosis to approximately $Z = 3.0$, beyond which it tapered down to zero. As the flow began to accelerate, the thickness of the separation zone was reduced along the tube in a wave-like manner starting from the edge of the stenosis. During this interval of the flow cycle, when the conditions for flow separation were least favourable, the thickness reached a minimum value of $0.25R$ within $Z < 2.0$ and the reattachment point moved upstream to about $Z = 2.8$. At about 65 ms into the acceleration phase ($T_{min} + 65$ ms) an almost uniform separation zone was seen with a normalized thickness of roughly $0.30R$ and the reattachment point fluctuated between $Z = 2.8$ and 4.5. Twenty five milliseconds later ($T_{max} - 75$ ms) the separation boundary began to move closer towards the vessel wall near $Z = 3.7$, until it eventually disappeared at $T_{max} - 45$ ms and, simultaneously, waves and streamwise vortices were generated in the high-shear layer at $Z = 1.4$. Transition to turbulence was triggered by the breakdown of these structures near $Z = 4.5$, the location that corresponded to the approximate position of the reattachment point. The turbulence generated in this manner lasted for about 140 ms, approximately 20 ms longer than that seen with the 65% stenosis. It should be noted that for the 75% stenosis there was insufficient time during the acceleration phase for complete flow relaminarization, in contrast to that observed for the 65% stenosis.

At any phase of the flow cycle the poststenotic flow field can be divided into four zones. While the velocity field in each zone depends on the time in the flow cycle, for convenience in discussion it is simplest to view the pattern in each zone during just two phases, namely, the turbulent generation and the relaminarization phase. Figure 15 illustrates the patterns observed in the four zones during the turbulent phase. From the motion pictures it was observed that the flow in the stable jet zone was

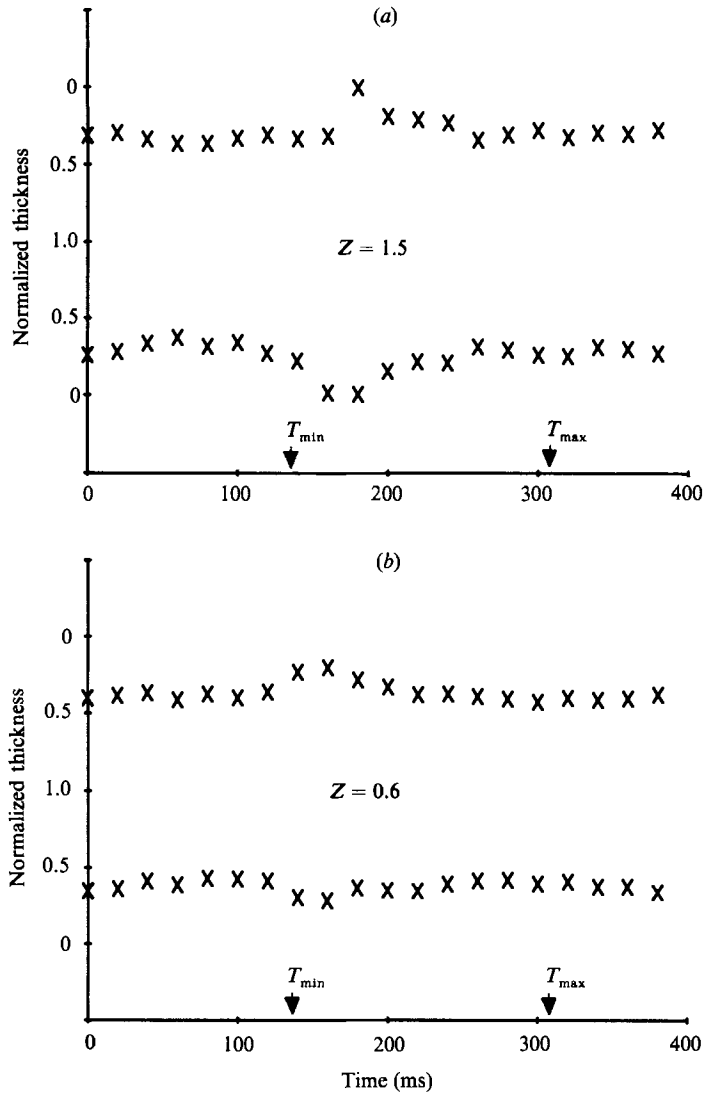

FIGURE 12. Time variation of the thickness of the separation zone for (*a*) the 65% stenosis at $Z = 1.5$; (*b*) the 75% stenosis at $Z = 0.6$.

three-dimensional and that the circumferential motion is quite significant during the turbulent generation phase. Also during this phase, three toroidal vortices appearing as typical Kelvin–Helmholtz vortex roll-ups can be seen extending axisymmetrically from $Z = 1.4$ to about $Z = 3.0$. Sometimes during this phase, wave motions were seen to be accompanied by the vortices. These patterns are partially shown in the $t = 280$ and 320 ms frames of both figures 10(*a*) and 10(*b*) as well as the last frame of figure 14. For the second zone (figure 15), which lies between $Z = 3.0$ and 4.5, the flow is in a transitional state throughout the cycle and it lacks symmetry. This lack of symmetry is more pronounced during the turbulent phase owing to the strong interaction between the jet and both the vortices and waves. Towards the end of this zone, breakdown of the coherent structures occurs and this leads to the third zone, where maximum turbulence occurs. The turbulence occupies the entire cross-section

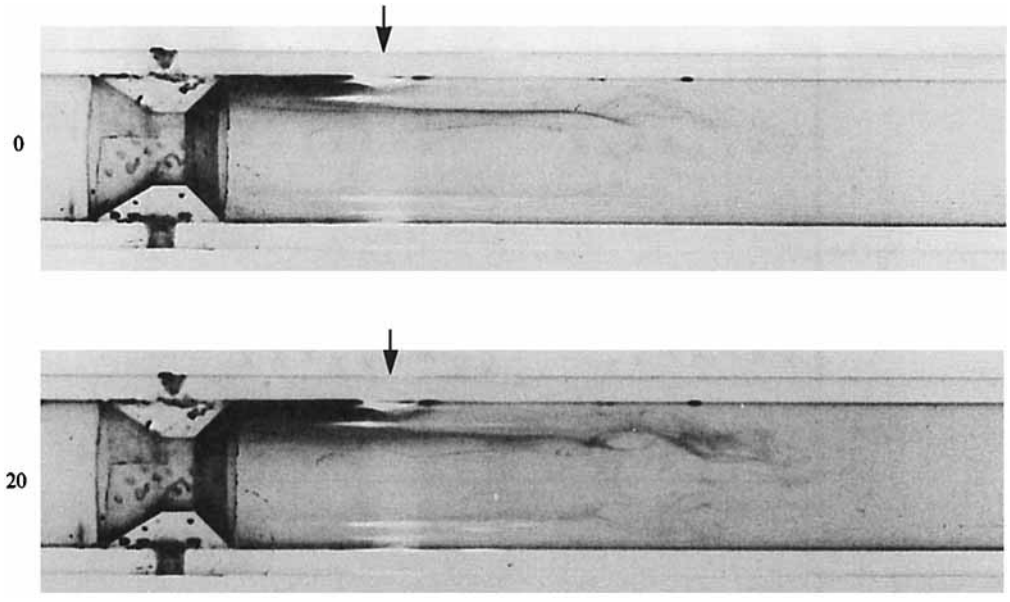

FIGURE 13. Photographs taken 20 ms apart, showing some features of the flow separation region just distal to the 75% stenosis. The top frame was taken 45 ms after peak flow. The arrows indicate the entry point of the radiation from the mercury lamp.

of the tube and extends downstream for about three tube diameters. As is clearly shown in figure 16, relaminarization occurs in the final zone at any instant in the flow cycle beyond $Z = 7.5$. The interface of maximum fluctuation of the axial velocity, especially in the wall region, lies between zones II and III, where breakdown of the jet flow through interaction with the waves and vortices occurs.

Initially, measurements of the wall shear stress for the 65% and 75% area stenoses were made using a 5.1 ms flash delay. Because of the turbulent nature of the flow, the traces were quite blurred and it was not possible to determine accurately the wall velocity gradient, especially in the vicinity of the reattachment point. In addition, since the gradients were seen to vary strongly with axial position and phase of the cycle, the flash delay was reduced to either 2.1 or 1.1 ms, as discussed earlier. Examples of the displacement profiles obtained with these two delays for the 75% stenosis are shown in figure 17. They indicate that large-scale eddies were more predominant in the upstream half of zone III. Table 2 shows the mean value of the wall shear stress and the fluctuation intensity, as measured by the range and standard deviation, based on twenty measurements for each position and phase in the flow cycle. The peak values of the shear stress are at least eight times higher than those measured upstream of the stenosis. The fluctuations reach a maximum at around $Z = 4.3$: the location that corresponds to the approximate position of the reattachment point. In the immediate vicinity of this point, flow in the wall region changes rapidly between positive and negative values, thereby causing large fluctuations in wall shear stress around a relatively small mean value. Furthermore, it should be noted that for any axial position the maximum intensity of the fluctuation of the wall shear stress occurred for about 40 ms after peak flow. This behaviour is expected since the effects of the decreasing (unfavourable) pressure gradient would be most intense shortly after peak flow, as was noted earlier for mild stenoses.

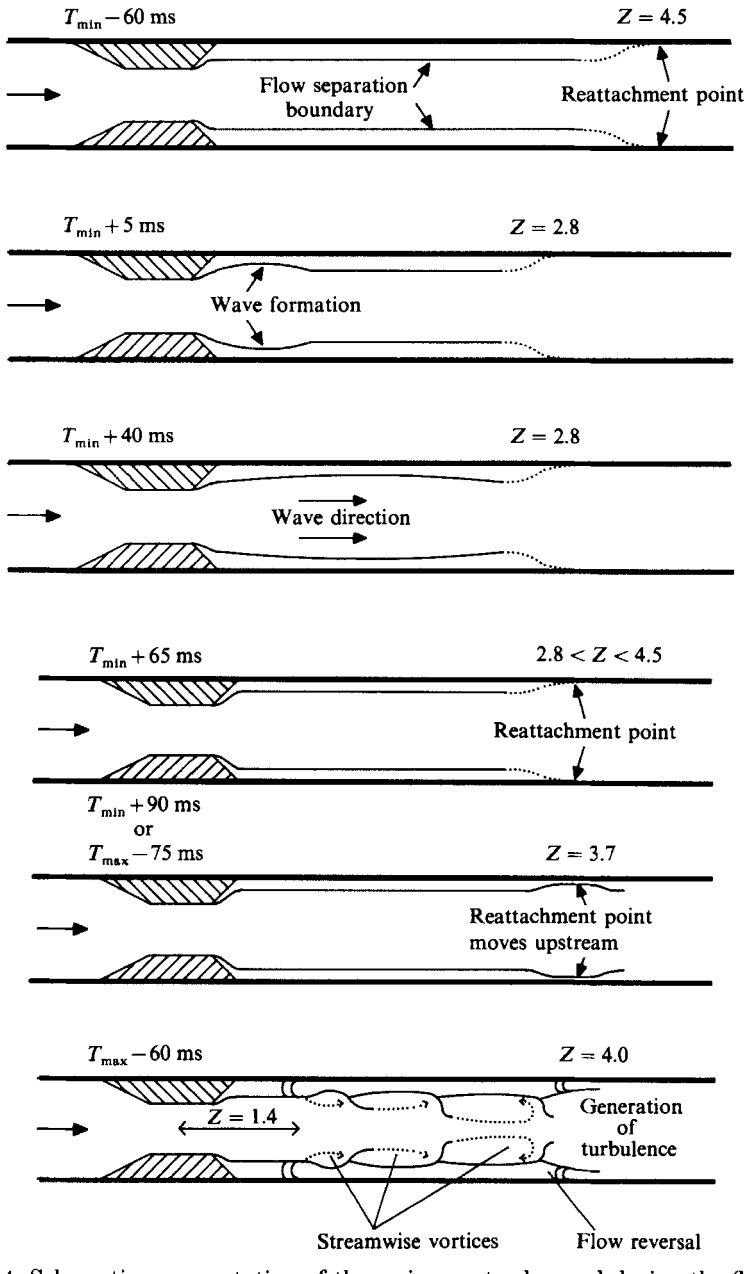

FIGURE 14. Schematic representation of the main events observed during the flow cycle downstream from the 75% stenosis.

4. Discussion

4.1. *Results*

Previous studies on pulsatile flow through mild streamlined stenoses have suggested that the vortical structures found in the downstream or poststenotic regions were shed from within the stenosis in the early acceleration phase (Ahmed & Giddens 1984; Lieber 1985). The evidence was based on observations of some disturbances

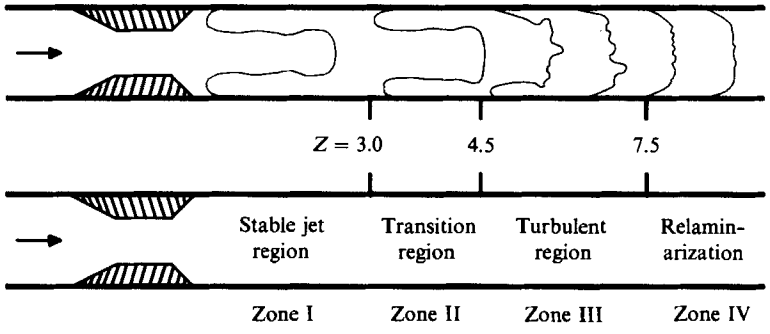

FIGURE 15. Schematic representations of the velocity field in the four poststenotic zones for the 75% stenosis during the vortex generation phase of the flow cycle.

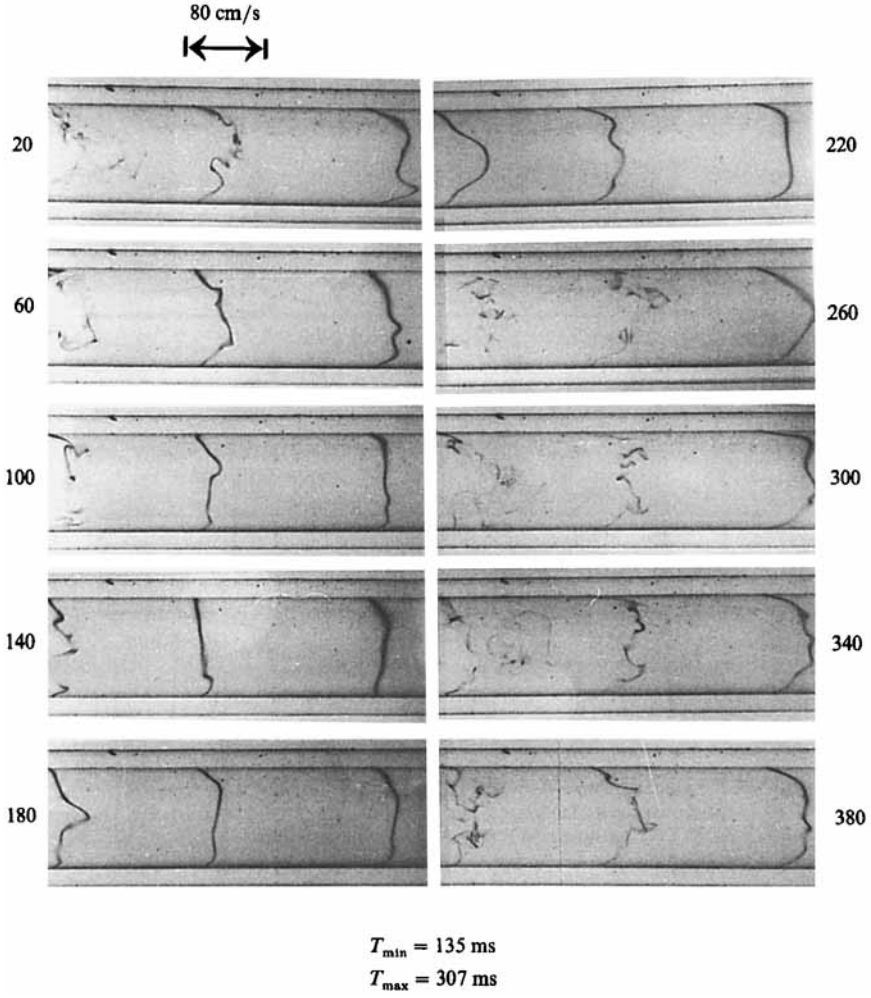

FIGURE 16. Selected photographs taken at 40 ms intervals throughout the flow cycle for the 75% stenosis. The flash delay was 5.1 ms and the traces are located at $Z = 4.2$, 5.6 and 7.5.

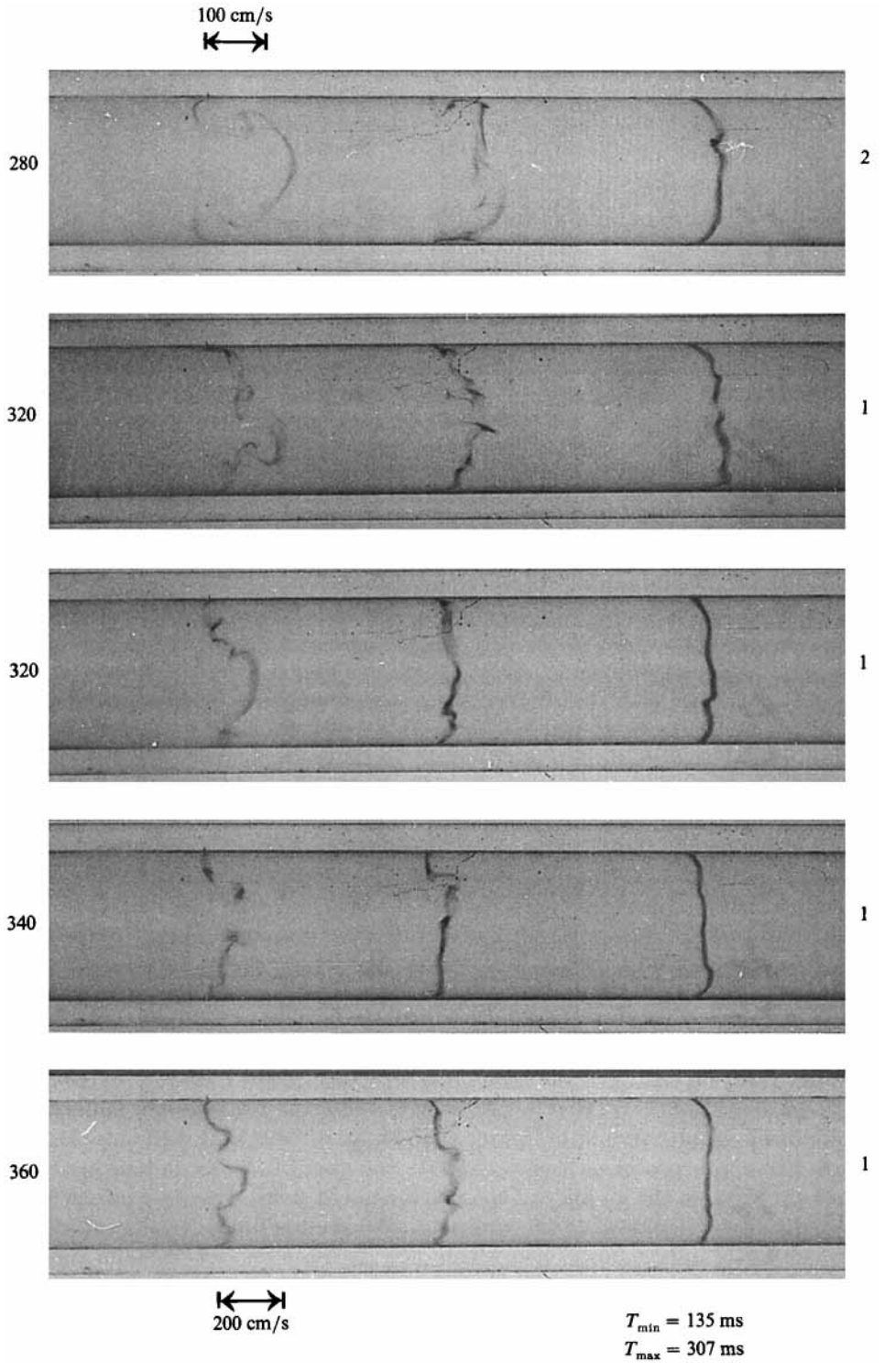

FIGURE 17. Selected photographs of the dye displacement profiles for the 75% area stenosis using flash delays of 1.1 and 2.1 ms (shown as 1 and 2 respectively) during the vortex generation phase of the flow cycle. The traces are positioned at $Z = 4.5$, 6.1, 7.8.

		Shear stress (dynes/cm^2)		
Time (ms)	Z	Mean	Range	Std dev
280	2.7	−6.0	−11.6–4.6	4.8
	4.3	−13.7	−55.6–26.2	20.3
	6.0	1.2	20.8–18.0	13.1
320	2.7	−28.3	−95.6–11.6	26.9
	4.3	2.1	−54.1–77.4	29.0
	6.0	23.4	6.0–49.7	11.8
360	2.7	−7.4	−12.8–2.5	3.6
	4.3	2.7	−17.8–35.8	14.9
	6.0	12.1	−1.0–24.6	8.8

TABLE 2. Measured wall shear stresses for flow through the 75% stenosis at different axial locations and times in the flow cycle, obtained using 1.1 and 2.1 ms flash delays

seen beyond $Z = 2.0$ through the use of hydrogen-bubble flow visualization, and also from fluctuations in the centreline velocities measured with LDA. However, the results of our study clearly indicate that these structures are formed during the early stages of the deceleration phase and in regions of either high shear or inflectional velocity profiles. This suggests that the structures identified in the previous studies during early acceleration are remnants of the disturbances formed in the deceleration phase of the previous cycle.

Ahmed & Giddens (1984) and Lieber (1985) have also studied the poststenotic wall shear stress patterns. They determined the phase-averaged wall shear stress by using a linear fit to the phase-averaged velocities obtained from LDA measurements made at several radial positions close to the wall. In order to compare their results with ours in a dimensionless manner, it is more convenient to use the ratio of the downstream to the upstream stresses rather than to use the friction factor as defined in the prior studies. For flow through a 75% streamlined stenosis and with $Re_m = 600$, $Re_{m\omega} = 400$ and $\alpha = 7.5$, Ahmed & Giddens (1984) reported that the transition to turbulence occurred just after peak flow at $Z = 6.0$ and that the magnitude of the phase-averaged wall shear stress within the turbulent region and at the reattachment point was approximately the same as in the upstream region. In addition, Lieber (1985) has shown that for flow through a 90%-area-reduction streamlined stenosis and with $Re_m = 600$, $Re_{m\omega} = 400$ and $\alpha = 5.3$, the transition to turbulence occurred just before peak flow near $Z = 6.0$ and the phase-averaged values reached a maximum value of about three times higher than those found upstream. Since Lieber's measurements appear to have been made in the viscous sublayer, the accuracy of his results should be better than those of Ahmed & Giddens. However, there are two major problems associated with the use of LDA for measuring the wall shear stress. First, in the vicinity of the reattachment point where we observed large fluctuations in the thickness of the viscous sublayer, it is difficult to ensure that the sample volume is always positioned within the viscous sublayer. Second, significant error can arise in attempting to determine a non-periodic velocity gradient using single-point, phase-averaged measurements. Our measurement technique avoids these problems since it measures instantaneous values that provide a much fuller description of the flow behaviour especially near the wall.

For steady flow through a 75%-area-reduction nozzle with an abrupt expansion, Iribarne *et al.* (1972) have shown that transition to turbulence was triggered at

$Re = 389$ and that the instantaneous value of the wall shear stress in the reattachment zone reached a value three times higher than the upstream value. This should be contrasted with our factor of eight for pulsatile flow through our more highly streamlined 65% and 75% stenoses. Consequently, it appears that there is an interaction between the imposed flow oscillation and the turbulence in the viscous sublayer. Furthermore, our results show that the strength of this interaction is greatest during early deceleration. The existence of a similar interaction in turbulent pulsatile pipe flow was demonstrated by Mao & Hanratty (1986), who also noted that such an interaction is not included in existing theories on turbulence.

4.2. *Evaluation of the photochromic method*

Since this study illustrates for the first time the use of a multiple-trace photochromic method for both quantitative and qualitative flow analysis, it is important to provide a brief assessment of its advantages and limitations.

The ability to determine the instantaneous velocity distributions at several sites simultaneously is of considerable value. First, the acquisition of velocity data is more efficient since a multiplicity of profiles are simultaneously recorded. Second, the display of the instantaneous axial velocity profiles at various sites in a selected section of the vessel provides a more complete description of the space–time relationship of the flow field. The visual impression gained in this manner along with velocity data can facilitate characterization of coherent structures such as turbulent bursts (Talmon *et al.* 1986) and turbulent plugs and patches (Stettler & Hussain 1986; Hussain 1986). In addition, the first and second partial derivatives (with respect to the radial position) of the axial velocity can be determined, provided sufficiently short flash delays are used. These quantities should provide useful guidance in making appropraite simplifying assumptions for numerical models.

Third, multiple traces help to identify the approximate position of the reattachment point by simply 'bracketing' its position. Understandably, using Eulerian-type measurement methods there is considerable uncertainity in its location and, in addition, measurement of the instantaneous wall shear stress in the vicinity of this point is quite difficult. As shown in this study, an inherent feature of the photochromic method is that it permits the velocity gradient to be measured regardless of the flow condition. Thus, by using multiple traces, we were able not only to determine the relative position of the reattachment point in turbulent flow, but also to measure the instantaneous wall shear stress in the nearby regions. Furthermore, in some of the photographs (e.g. figure 9, frame = 60 ms), the 0.2 mm trace was split in the vicinity of the reattachment point and both the forward and revese flow velocity gradients were seen, thereby indicating that the reattachment point is well defined.

Additional advantages of the photochromic method arise from its non-invasive nature and from the ease in generating the trace at any location in the duct and at any instant of the cycle. In addition, since both the photochromic indicator and the resultant dye are in true solution and have a molecular weight comparable with the solvent, the trace indicates the true movement of the fluid both with regard to structures such as vortices of any size and to molecular diffusion. There can be no misrepresnetation of flow structures as has been reported for flow markers such as hydrogen bubbles, injected dyes and smoke particles (Hussain 1986). Some limitations of the photochromic method can arise from the fact that the indicator used in our study requires the test fluid be organic and that the flow duct be reasonably transparent at around 337 nm. However, these limitations could be

overcome by using water-soluble indicators (Fogwell & Hope 1988) and indicators that can be activated at longer wavelengths (Cloitre & Chauveau 1983). In common with other flow visualization techniques, the photochromic method involves considerable effort in the photography and analysis. Evidently, these could be reduced by using video camera digital recording and image processing.

In the present study attention has been focused on the axial velocity. However, for two-dimensional flow, it should be noted that the radial velocity can be determined from a measurement of the axial velocity through the use of the continuity equation. This has been demonstrated by Seeley *et al.* (1975) for laminar flow around a sphere and by Davis *et al.* (1985) for flow during bubble formation. Also, Davis *et al.* (1985) have shown that two-dimensional Lagrangian velocity data, that are otherwise difficult to obtain, can be recorded by using intersecting traces and following the points of intersection. These data, along with the continuity equation, can be used to calculate the remaining (third-dimension) velocity component. Alternatively, by photographically recording the motion of the intersection points in two planes, the velocity vector at each point can be determined. For the measurement of velocity gradients, a general discussion of the limitations and advantages of various methods has been presented by Wallace (1986). He points out that the use of a photochromic tracer grid in the manner developed by D'Arco, Charmet & Cloitre (1982) and Charmet, Ferminger & Jennfer (1984) allows the velocity gradients to be measured directly, thereby enabling the vorticity to be determined. Furthermore, it should be noted that the use of one or more viewing mirrors would provide information on motions outside the normal viewing plane.

We especially thank Larry Mo, Weimin Chen and Dr Y. F. Law for assistance in various phases of this work, and Professor Ross Ethier for reviewing the manuscript. In addition, the financial support of the Medical Research Council and the Natural Sciences and Engineering Research Council of Canada is gratefully acknowledged.

REFERENCES

AHMED, S. & GIDDENS, D. P. 1984 Pulsatile poststenotic flow studies with laser Doppler anemometry. *J. Biomech.* **17**, 695–705.

BARNES, R. W., BONE, G. E., REINERSON, J. E., SKYMAKER, F. E. & HOKENSON, D. E. 1976 Non-invasive ultrasound carotid arteriography: Prospective validation by constrast arteriography. *Surgery* **80**, 328–335.

CHARMET, J. C., FERMINGER, M. & JENNFER, P. 1984 Visualization d'ecoulement et mesure de gradient de vitesse par des traceurs photochromes. *C. R. Acad. Sci. Paris* **298**, 103–106.

CLOITRE, M. & CHAUVEAU, J. 1983 Metal dithizonate for flash photolysis applications in hydrodynamics. *Optics Comm.* **47**, 42–46.

D'ARCO, A., CHARMET, J. C. & CLOITRE, M. 1982 Nouvelle technique de marquage d'ecoulment par utilisation de molecules photochromes. *Rev. Phys. Appl. Paris* **17**, 89–93.

DAVIS, J., BOTTCHER, J., JOHNSON, G. & MARSCHALL, E. 1985 Photochromic flow visualization in single-phase and two-phase flows. In *Intl. Symp. on Physical and Numerical Flow Visualization, Albuquerque, New Mexico* (ed. M. L. Billet, J. H. Kim & T. R. Heidrick), pp. 75–79, ASME.

DUNN, S. G. & SMITH, J. W. 1972 Some statistical properties of turbulent momentum transfer in rough pipes. *Can. J. Chem. Engng* **50**, 561–568.

FOGWELL, T. W. & HOPE, C. B. 1988 Photochromic dye tracing in water flows. (Submitted for publication.)

GAVER, D. P. III & GROTBERG, J. B. 1986 An experimental investigation of oscillatory flow in a tapered channel, *J. Fluid. Mech.* **172**, 47–61.

HANLE, D. D., HARRISON, E. C., YOGANATHAN, A. P. & CORCORAN, W. H. 1987 Turbulence downstream from the Ionescu-Shiley bioprosthesis in steady and pulsatile flow. *Med. Biol. Engng & Comput.* **25**, 645–649.

HINO, M., SAWAMOTO, M. & TOKASU, S. 1976 Experiments on transition to turbulence in an oscillatory pipe flow. *J. Fluid Mech.* **75**, 193–207.

HUSSAIN, A. K. M. F. 1986 Coherent flow structures and turbulence. *J. Fluid Mech.* **173**, 303–356.

IRIBARNE, A., FRANTISAK, F., HUMMEL, R. L. & SMITH, J. W. 1969 Transition and turbulent flow parameters in a smooth pipe by direct flow visualization. *Chem. Engng Prog. (Symp. Ser.)* **65**, 60–70.

IRIBARNE, A., FRANTISAK, F., HUMMEL, R. L. & SMITH, J. W. 1972 An experimental study of instabilities and other flow properties of a laminar pipe jet. *AIChE J.* **18**, 689–698.

JOHNSTON, K. W., BAKER, W. H., BURNHAM, S. J., HAYES, A. C., KUPPER, C. A. & POOLE, M. A. 1986 Quantitative analysis of continuous-wave Doppler spectral broadening for the diagnosis of carotid disease: results of a multicenter study. *J. Vasc. Surg.* **4**, 493–504.

KONDRATAS, H. M. & HUMMEL, R. L. 1980 Application of the photochromic tracer technique for flow visualization near the wall region. In *Flow visualization III, Michigan* (ed. W. Merzkirch), pp. 387–391, Hemisphere.

KU, D. N. & GIDDENS, D. P. 1987 Laser Doppler anemomentry measurements of pulsatile flow in a model carotid bifurcation. *J. Biomech.* **20**, 407–431.

LIEBER, B. 1985 Order and random structures in pulsatile flow through constricted tubes. Ph.D. thesis, Georgia Institute of Technology, Atlanta.

MAO, Z.-X. & HANRATTY, T. J. 1986 Studies of the wall shear stress in turbulent pulsatile pipe flow. *J. Fluid Mech.* **170**, 545–564.

OJHA, M. 1987 An experimental investigation of pulsatile flow through modelled arterial stenoses. Ph.D. thesis, University of Toronto.

OJHA, M., HUMMEL, R. L., COBBOLD, R. S. C. & JOHNSTON, K. W. 1988 Development and evaluation of a high resolution photochromic dye method for pulsatile flow studies. *J. Phys. E: Sci. Instrum.* **21**, 998–1004.

POOTS, J. K., COBBOLD, R. S. C., JOHNSTON, K. W., APPUGLIESE, R., KASSAM, M., ZEUCH, P. E. & HUMMEL, R. L. 1986*a* A new pulsatile flow visualization method using a photochromic dye with application to ultrasound. *Ann. Biomed. Engng* **14**, 203–218.

POOTS, J. K., JOHNSTON, K. W., COBBOLD, R. S. C. & KASSAM, M. 1986*a* Comparison of continuous wave Doppler ultrasound spectra with the spectra derived from a flow visualization model. *Ultrasound Med. Biol.* **12**, 125–133.

POPOVICH, A. T. & HUMMEL, R. L. 1967 A new method for non-disturbing turbulent flow measurements close to a wall. *Chem. Engng Soc.* **22**, 21–25.

RAMAPRIAN, B. R. & TU, S. W. 1980 An experimental study of oscillatory pipe flow at transitional Reynolds numbers. *J. Fluid Mech.* **100**, 513–544.

RAMAPRIAN, B. R. & TU, S. W. 1983 Fully developed periodic turbulent pipe flow. *J. Fluid Mech.* **137**, 59–81.

SEELEY, L. E., HUMMEL, R. L. & SMITH, J. W. 1975 Experimental velocity profiles in laminar flow around a sphere at intermediate Reynolds numbers. *J. Fluid Mech.* **68**, 591–608.

SHEMER, L., WYGNANSKI, I. & KIT, E. 1985 Pulsating flow in a pipe. *J. Fluid Mech.* **153**, 313–337.

SMITH, J. W. & HUMMEL, R. 1973 Studies of fluid flow by photography using a non-disturbing light sensitive indicator. *J. Soc. Mot. Pic. Tel. Engng* **83**, 278–281.

STETTLER, J. C. & HUSSAIN, A. K. M. F 1986 On transition of pulsatile pipe fow. *J. Fluid Mech.* **170**, 169–197.

TALMON, A. M., KUNEN, J. M. G. & OOMS, G. 1986 Simultaneous flow visulaization and Reynolds stress measurements in a turbulent boundary layer. *J. Fluid Mech.* **163**, 459–478.

THOMAS, L. C. 1980 The surface rejuvenation model of wall turbulence: Inner laws for U^+ and T^+. *Intl J. Heat Mass Transfer* **23**, 1099–1104.

WALLACE, J. M. 1986 Methods for measuring vorticity in turbulent flows. *Exp. Fluids.* **4**, 61–71.

WOMERSLEY, J. R. 1955 Method for the calculation of velocity, rate of flow and viscous drag in arteries when the pressure gradient is known. *J. Physiol.* **127**, 553–563.

YOGANATHAN, A. P., CORCORAN, W. H. & HARRISON, E. C. 1979 In vivo velocity measurements in the vicinity of aortic prostheses. *J. Biomech.* **12**, 135–152.